Realization of electronically tunable voltage-mode/current-mode quadrature sinusoidal oscillator using ZC-CG-CDBA

Dalibor Biolek [1,a,b], Abhirup Lahiri [c,*], Winai Jaikla [d], Montree Siripruchyanun [e], Josef Bajer [b]

[a] Department of Microelectronics, Brno University of Technology, Technicka 10, Brno, Czech Republic
[b] Department of EE, University of Defence Brno, Kounicova 65, Brno, Czech Republic
[c] 36-B, J and K Pocket, Dilshad Garden, Delhi-110095, India.
[d] Electric and Electronic Program, Faculty of Industrial Technology, Suan Sunandha Rajabhat University, Bangkok, Thailand
[e] Department of Teacher Training in Electrical Engineering, Faculty of Technical Education, King Mongkut's University of Technology North Bangkok, Bangkok, Thailand

ARTICLE INFO

ABSTRACT

This paper presents a first of its kind canonic realization of active RC (ARC) sinusoidal oscillator with non-interactive/independent tuning laws, which simultaneously provides buffered quadrature voltage outputs and explicit quadrature current outputs. The proposed circuit is created using a new active building block, namely the Z-copy controlled-gain current differencing buffered amplifier (ZC-CG-CDBA). The circuit uses three resistors and two grounded capacitors, and provides independent/non-interactive control of the condition of oscillation (CO) and the frequency of oscillation (FO) by means of different resistors. Other advantageous features of the circuit are the inherent electronic tunability of the FO via controlling current gains of the active elements and the suitability to be employed as a low-frequency oscillator. A non-ideal analysis of the circuit is carried out and experimental results verifying the workability of the proposed circuit are included.

1. Introduction

It is well known that any active RC sinusoidal oscillator providing independent control of the condition of oscillation (CO) and the frequency of oscillation (FO) requires the use of at least three resistors and two capacitors [1]. This particular set of 3R-2C oscillators (often also called canonic oscillators) has been researched extensively using various active building blocks like second-generation current conveyor (CCII) and current feedback operational amplifier (CFOA) (see [2–4] and the references cited therein). It is worth mentioning here that although many of the CFOA-based realizations in [3] could provide buffered quadrature voltage outputs (as also pointed out in Ref. [1] of [3]), their availability was not investigated in several subsequent realizations, and very recently a new CFOA-based single-resistance controlled (SRC) voltage-mode quadrature oscillator has been reported in [5]. Canonic 3R-2C voltage-mode quadrature oscillators (with buffered voltage outputs) employing current differencing buffered amplifier (CDBA) have also been proposed in [6, 7]. In [8], the authors propose SRC oscillators based on a single CDBA but with floating passive components and without the possibility of using

quadrature outputs. A CDBA-based SRC quadrature oscillator (QO) is proposed in [9]. However, this topology, containing four resistors and two grounded capacitors, is not canonic.

In view of the recent interest in current-mode signal processing, researchers have also come up with ingenious schemes of current-mode quadrature oscillators providing current outputs from high-impedance output terminals for explicit utilization, see [10–13] and references cited therein. In [14], the authors propose a collection of SRC oscillators with one or two high-impedance current outputs, each of them employing two differential difference complementary current conveyors (DDCCCs), two grounded capacitors, and two grounded resistors. However, owing to the oscillator topology, the phase shift between the output currents is not 90°, and thus these circuits cannot serve as quadrature oscillators. In addition, both the phase shift and the ratio of the magnitudes of generated waveforms change with the frequency of oscillation. Voltage low-impedance outputs are available only with the use of additional buffers. It is also seen that, the dynamic range of the frequency tuning is low since this frequency is indirectly proportional to the root of the controlling resistance. This tuning law also leads to the fact that for low-frequency oscillation, large values of resistances and capacitances are required. The authors of the paper [14] also propose several oscillator topologies in [15], each of them using two CFOA elements. However, floating resistors and capacitors are present in the circuits, and also these circuits cannot work as quadrature oscillators. The recently reported economical current-output SRC

* Corresponding author.
   E-mail addresses: dalibor.biolek@unob.cz (D. Biolek),
lahiriabhirup@yahoo.com (A. Lahiri), winai.ja@ssru.ac.th (W. Jaikla),
mts@kmutnb.ac.th (M. Siripruchyanun).
   [1] Tel.: +420 603363136; fax: +420 973443773.

oscillator in [16] employs only one ZC-CDTA (Z-copy current differencing transconductance amplifier), two grounded capacitors, and two pseudo-grounded resistors, with the possibility of adjusting the oscillation condition electronically via the internal transconductance of CDTA. However, this circuit provides only a single current output.

The above described state-of-the-art brings us to the problem of devising a quadrature oscillator which can simultaneously provide both buffered quadrature voltage outputs and explicit quadrature current outputs and thus be suitable for use as a sinusoidal input source for both voltage- and current-mode applications. The tuning law of this oscillator should be designed with the aim of avoiding the above problems. This problem was first formulated by Lahiri [13] and later attempted by Bajer and Biolek in [17]. The circuit in [17] uses a newly proposed building block, namely the Z-copy controlled-gain current differencing buffered amplifier (ZC-CG-CDBA) [18]. Since the ZC-CG-CDBA has multiple current copy terminals (which facilitate explicit current outputs) and a voltage buffer (which provides low-impedance voltage output); it is an ideal fit for devising a dual-mode quadrature oscillator. However, the circuit [17] uses four resistors and two capacitors and is not canonic.

In this paper, a new circuit topology of realizing 3R-2C dual-mode quadrature oscillators is reported, using two ZC-CG-CDBAs. This topology profits from several advantages of the ZC-CG-CDBA element in comparison with CCII- and CFOA-based oscillators. CCII and CFOA cannot offer the possibility of electronic control of their parameters, which would affect the FO. As a result, the CCII- and CFOA-based oscillators are controlled via external resistors. This is associated with several problems, for example with the problematic implementation of low-frequency oscillators. In this sense, ZC-CG-CDBA is more universal: it enables the same but, as an added value, the "alpha" method of electronic tuning is possible (Section 2). Another problem is due to the asymmetrical input stages of CCII and CFOA. CDBA has bipolar current inputs, allowing an easy and simultaneous implementation of positive and negative feedback, which is necessary for this type of oscillator structure. For CCII-based oscillators, both feedback signals must be implemented only via replacing the single current output by bipolar z+ and z− outputs, which represents a more complicated IC structure.

Analogously to [9], the proposed circuit structure is similar to the "lossless and lossy integrator in loop," and the lossless integrator is achieved via current injection to the n input of CDBA no. 2 from the Z-copy current output of CDBA no. 1 (this trick can be used only due to the oscillator synthesis based on the Z-copy attribute of novel ZC-CDBA). As a result, the oscillation condition does not depend on the "alpha-factors" of CDBAs, and both of the gains can be used for FO modification without disturbing CO. This results in a better performance of the oscillator in comparison with other circuits, particularly the current-mode SRC oscillators in [14]. The CO and FO can be set independently by two different resistors. Moreover, comparing the proposed oscillator with the non-canonic circuit in [9], there are four additional features: (1) The FO is electronically tunable by means of current gains. (2) Not only voltage but also current outputs are available. (3) The circuit is also suitable to be used as a low ω_o sensitivity low-frequency oscillator. (4) If the tuning law from (1) is used, then the dynamic range of the FO tuning is wider than for conventional SRC oscillators, with a fixed ratio of the amplitudes of generated waveforms during the FO tuning.

In order to verify the workability of the proposed circuit, an oscillator specimen was constructed via commercial integrated circuits, and a combination of measurements and SPICE simulations were performed.

The paper is organized as follows: In Section 2, which follows this introduction, the proposed voltage- /current-mode quadrature oscillator employing two ZC-CG-CDBAs is described, and the CO and

FO as well as the proof of the orthogonality of generated waveforms are derived here. Section 3 deals with detailed error analysis, which investigates the impact of the active component imperfections and parasitic impedances on the CO, FO, and on the phase error of the quadrature signals. Section 4 contains experimental results of measurements carried out on an oscillator specimen, which was fabricated based on the so-called diamond transistors OPA860, with some data post-processing in PSpice, which also enabled an effective comparison of the measured results with the results predicted via error analysis.

Note that, as it is usual with RC oscillators, the oscillation frequency depends indirectly on two resistances and two capacitances of the working resistors and capacitors, and their non-zero temperature coefficients are indeed important sources of FO variation with temperature. That is why low-temperature-coefficient resistors and capacitors were used for the oscillator specimen. Other techniques of frequency calibration may be employed for increasing the frequency accuracy in order to compensate for the systematic device variation and for slow-changing phenomena such as temperature variation, but this is not the main topic of interest here.

This paper does not focus on the phase noise of oscillators although it is certainly very important for high frequency oscillators used for communication circuits like frequency synthesizers based on phase-locked loops. The phase noise study of the proposed oscillator may be addressed in a future communication after prospective on-chip implementation of the oscillator, which enables shifting the FO to the above high-frequency region.

2. Proposed circuit

The Z-copy controlled gain current differencing buffered amplifier (ZC-CG-CDBA) [18] consists of a low-impedance CDU (Current Differencing Unit) [19], CCF (Controlled Current Follower), and a unity-gain voltage buffer [19]. The difference of currents I_p and I_n flows to the CCF being available also at zc (Z-copy) terminals. The number of these zc terminals, as well as the directions of these terminal currents can be chosen arbitrarily, depending on the need of a concrete application. CCF operates as a current attenuator, multiplying its input current by transfer α ($0 < \alpha \le 1$) and providing its output current to the z terminal. The characteristic equations for ZC-CG-CDBA according to [17,18] are given as

$$V_p = V_n = 0, \quad I_{zc} = I_p - I_n, \quad I_z = \alpha I_{zc}, \quad V_w = V_z \tag{1}$$

The circuit symbol of ZC-CG-CDBA and its behavioral model are shown in Fig. 1(a) and (b). A possible implementation of ZC-CG-CDBA is provided in [18].

The ZC-CG-CDBA-based dual-mode sinusoidal oscillator is shown in Fig. 2. Note that active component no. 1 provides two zc terminals, one for leading the current to the n input of CDBA no. 2, and the other serves as the current output. Using (1) and doing routine circuit analysis yields the following characteristic equation:

$$s^2 C_1 C_2 R_1 R_2 + \alpha_2 s C_1 R_1 R_2 \left(\frac{1}{R_1} - \frac{1}{R_3} \right) + \alpha_1 \alpha_2 = 0 \tag{2}$$

From (2), the CO is given as

$$R_1 \ge R_3 \tag{3}$$

and the FO is as follows:

$$f_0 = \frac{1}{2\pi} \sqrt{\frac{\alpha_1 \alpha_2}{C_1 C_2 R_1 R_2}} \tag{4}$$

It is evident from (3) and (4) that for fixed values of the passive components, the CO and the FO are independently controlled by means of resistors R_3 and R_2, respectively. Thus, the oscillator can
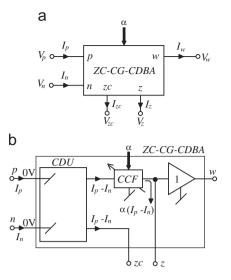
Fig. 1. ZC-CG-CDBA [18]: (a) schematic model and (b) behavioral model.
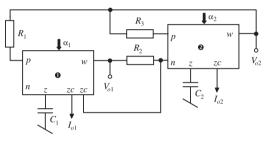

Fig. 2. Voltage-/current-mode quadrature oscillator using two ZC-CG-CDBAs.

be classified as a "single-resistance-controlled oscillator" or SRCO in short.

All terminals of the three resistors in the circuit in Fig. 2 are connected between two low-impedance nodes, namely between the w-output of active element (output of voltage buffer) and the p- or the n-terminal (controlling nodes of the CDU). As a result, one terminal of each resistor is pseudo-grounded (it has a ground potential), and the potential parasitic impedances are thus eliminated in a similar way as for grounded terminals. In addition, R_3 can be implemented as an electronically controlled drain-source resistance via the MOS transistor structure with its source terminal pseudo-grounded. The gate voltage, rectified from the generated waveforms, can control the resistance R_3 such that the CO is automatically fulfilled. Another possible method of the automatic gain control is, for example, to implement R_3 as a part of opto-coupler [20].

An interesting feature of the circuit is the electronic control of FO by means of current gains α_2 and α_1. Such inherent tunability is not available in any current-conveyor-based SRCO (for a list of building blocks classified under current-conveyor family refer to [19]). Also, since α_1, $\alpha_2 \leq 1$, the circuit can be used to generate lower frequency sinusoids for given passive component values as compared to SRCOs governed specifically by tuning laws provided in (1) and (2) of [21]. Thus, α_2 and/or α_1 can be regarded as reducing factors which reduce the oscillation frequency ω'' to ω_o. This is unlike the low-frequency oscillator circuits in [21], which have a frequency-reducing factor of the form of $\Delta\omega = \omega_o/\omega'' = \sqrt{1-n}$, and thus yield a high sensitivity value $S_n^{\omega_o}$ (as pointed out in [22]). Frequency reducing factors of the form of $\sqrt{k}$ (as in our case) are thus preferred and they provide a fixed and low ω_o sensitivity value ($= 0.5$). Tuning the FO by $\alpha_1 = \alpha_2 = \alpha$, although it increases the ω_o sensitivity value ($S_\alpha^{\omega_o} = 1$), provides a higher dynamic range of control than by either α_1 or α_2.

The two explicit quadrature current outputs from the high output impedance zc terminals are shown in Fig. 2, and are related as

$$\frac{I_{o2}}{I_{o1}} = j\omega_0 \frac{C_2 R_1}{\alpha_2} = j\sqrt{\frac{\alpha_1}{\alpha_2} \frac{R_1}{R_2} \frac{C_2}{C_1}} \tag{5}$$

and the marked quadrature voltages from the low output impedance w terminals are related as

$$\frac{V_{o2}}{V_{o1}} = j\omega_0 \frac{C_1 R_1}{\alpha_1} = j\sqrt{\frac{\alpha_2}{\alpha_1} \frac{R_1}{R_2} \frac{C_1}{C_2}} \tag{6}$$

Note from (4) from (6) that if

$$R_1 = R_2 = R, \quad C_1 = C_2 = C, \quad \alpha_1 = \alpha_2 = \alpha \tag{7}$$

then

$$f_0 = \frac{1}{2\pi} \frac{\alpha}{CR}, \quad \frac{I_{o2}}{I_{o1}} = \frac{V_{o2}}{V_{o1}} = j \tag{8}$$

The oscillation frequency will be directly proportional to the current gain α and indirectly to the C and R values, with equal magnitudes of both quadrature voltage and current signals.

3. Non-ideal analysis

The proposed QO is analyzed for the following ZC-CG-CDBA non-idealities:

- Considering the ith ZC-CG-CDBA (where $i = 1, 2$), α_{p_i} and α_{n_i} represent the current transfer gains from the p_i and the n_i terminals to the z_i terminal, respectively. They can be represented as $\alpha_{p_i} = \alpha_i(1-\varepsilon_{p_i})$, $\alpha_{n_i} = \alpha_i(1-\varepsilon_{n_i})$, where ε_{p_i} and ε_{n_i} are the current tracking errors and ideally are zero-valued. Similarly, α_{pc_i} and α_{nc_i} represent the current transfers from p and n to the zc terminal of ZC-CG-CDBA no. i, being one in the ideal case. Also, let us denote β_i the voltage transfer gain from the z_i to the w_i terminal, whose value is ideally one.
- In addition, the parasitic terminal impedances of ZC-CG-CDBAs will take effect. The most dominant of them are analyzed in [18]: The input resistances of the p_i and n_i terminals R_{p_i} and R_{n_i}, the resistances and capacitances of the z_i terminal R_{z_i}, C_{z_i}, and of the z_c terminal of ZC-CG-CDBA no. 1, R_{zc}, C_{zc}.
- An analysis of the circuit in Fig. 2 shows that the influence of parasitic capacitance C_{zc} is negligible if the additional cut off frequency

$$\omega_{cof} = \frac{1}{C_{zc}} \left(\frac{1}{R_{n_2}} + \frac{1}{R_{zc}} + \frac{1}{R_2} \right) \approx \frac{1}{C_{zc} R_{n_2}} \tag{9}$$

which is caused by this capacitance, is much higher than the oscillation frequency. Note that this condition is perfectly fulfilled in a real circuit since the working capacitances and resistances, which determine the oscillation frequency, are designed much higher than the parasitic values C_{zc} and R_{n_2}.

Considering the above model of active elements and taking (9) into account, the modified FO and CO become
FO:

$$\omega_o'^2 = \frac{1}{C_1' C_2' R_{z_1} R_{z_2}} - \frac{\alpha_{p_2} \beta_2}{C_1' C_2' R_{z_1} R_3'}$$
$$+ \frac{\alpha_{n_2} \beta_2}{C_1' C_2' R_1' (R_2' + R_2(R_{n_2}/R_{zc}))} \left(\alpha_{pc_1} \frac{R_2}{R_{z_1}} + \alpha_{p_1} \beta_1 \right) \tag{10}$$

CO:

$$\frac{R_1'}{R_3'} \geq \frac{\alpha_{n_2}}{\alpha_{p_2}} \frac{\alpha_{pc_1}}{1 + (R_{n_2}/R_2) + R_{n_2}/R_{zc}} + \frac{1}{\alpha_{p_2} \beta_2} \left(\frac{R_1'}{R_{z_2}} + \frac{C_2'}{C_1'} \frac{R_1'}{R_{z_1}} \right) \tag{11}$$

where

$$R'_1 = R_1 + R_{p_1}, \quad R'_2 = R_2 + R_{n_2}$$
$$R'_3 = R_3 + R_{p_2}, \quad C'_1 = C_1 + C_{z_1}, \text{ and } \quad C'_2 = C_2 + C_{z_2} \tag{12}$$

It should be easy to show that (10) and (11) pass to (2) and (3) when designing the capacitances and resistances of external capacitors and resistors such that the parasitic elements will have a negligible effect, and when all current and voltage gains tend to their ideal values.

Considering the real relations between the parameters of passive components and the parasitic values yields that the dominant term on the right hand side of (10) is the last one, and that

$$\omega'_0 \approx \sqrt{\frac{\alpha_{p_1}\beta_1\alpha_{n_2}\beta_2}{C'_1 C'_2 R'_1 R'_2}} \tag{13}$$

In comparison to the theoretical value (4), the oscillation frequency is decreased due to the influence of parasitic resistances R_{p_1} and R_{n_2}, which virtually increase resistances R_1 and R_2, and also due to the influence of parasitic capacitances C_{z_1} and C_{z_2}, which virtually increase working capacitances C_1 and C_2. Other modifications of the frequency are due to the non-ideal values of current and voltage gains in the numerator of (13).

Eq. (10) is more general and can be used for error analysis if the parameters of passive components are designed near the values of parasitic elements.

Similarly, (11) can be simplified, considering $R'_1 \ll R_{z_1}$, $R'_1 \ll R_{z_2}$, $R_{n_2} \ll R_{zc}$:

$$\frac{R'_1}{R'_3} \geq \frac{\alpha_{n_2}}{\alpha_{p_2}} \frac{\alpha_{pc_1}}{1 + (R_{n_2}/R_2)} \tag{14}$$

For maintaining the oscillations, the ratio of the left-hand side resistances, which is of unit value in the ideal case, is decreased due to the influence of nonzero resistance R_{n_2}, and it is also modified by tracking errors of the current gains of the second ZC-CG-CDBA, and by the non-ideal gain of the current mirror providing current I_{zc} of ZC-CG-CDBA no. 1. It should be noted that the choice $R_2 \gg R_{n_2}$ ensures that the CO will not be violated by a potential FO control via R_2.

In quadrature oscillators, the effect of the above parasitics on the phase shifts between the generated waveforms need to be analyzed. Tedious derivations lead to the following generalizations of Eqs. (5) and (6):

$$\frac{I'_{o2}}{I'_{o1}} = \frac{R'_1}{\beta_2 \alpha_{pc_1} \alpha_{n_2}} \left[\alpha_{nc_2} \left(\frac{1}{R_{z2}} + j\omega'_0 C'_2 \right) - \frac{\beta_2}{R'_3} (\alpha_{nc_2}\alpha_{p_2} - \alpha_{pc_2}\alpha_{n_2}) \right] \tag{15}$$

$$\frac{V'_{o2}}{V'_{o1}} = \frac{R'_1}{\beta_1 \alpha_{p_1}} \left(\frac{1}{R_{z1}} + j\omega'_0 C'_1 \right) \tag{16}$$

Eq. (15) shows two possible reasons for the variation of the phase shift of current outputs from the ideal value of 90°:

1. Violation of the following symmetry of current gains of ZC-CG-CDBA no. 2:

$$\alpha_{nc_2}\alpha_{p_2} = \alpha_{pc_2}\alpha_{n_2}, \quad \text{or} \quad \frac{\alpha_{p_2}}{\alpha_{n_2}} = \frac{\alpha_{pc_2}}{\alpha_{nc_2}} \tag{17}$$

2. The existence of the finite value of parasitic resistance R_{z2} in parallel to capacitor C_2, which modifies the 90° phase shift.

The error angle δ_I, i.e. the variation of the real phase shift between output currents from 90°, is derived from Eq. (15) as follows:

$$\delta_I = \tan^{-1} \left[\frac{1}{\omega'_0 C'_2 R_{z2}} - \beta_2 \alpha_{n_2} \frac{(\alpha_{p_2}/\alpha_{n_2}) - (\alpha_{pc_2}/\alpha_{nc_2})}{\omega'_0 C'_2 R'_3} \right] \tag{18}$$

Similarly, Eq. (16) shows that the phase shift between the voltage output signals can decline from the value 90° due to the finite value of parasitic resistance R_{z1}, which causes the error angle δ_V:

$$\delta_V = \tan^{-1} \left[\frac{1}{\omega'_0 C'_1 R_{z1}} \right] \tag{19}$$

Assuming conditions (7) and using simplified assumptions leading to Eqs. (13) and (14), the error angles can roughly be estimated as follows:

$$\delta_I \approx \tan^{-1} \left[\frac{R}{R_{z2}} \frac{1}{\sqrt{\alpha_{p_1}\alpha_{n_2}\beta_1\beta_2} - \left(\frac{\alpha_{p_2}}{\alpha_{n_2}} - \frac{\alpha_{pc_2}}{\alpha_{nc_2}} \right) \sqrt{\frac{\alpha_{n_2}\beta_2}{\alpha_{p_1}\beta_1}}} \right] \tag{20}$$

$$\delta_V \approx \tan^{-1} \left[\frac{R}{R_{z1}} \frac{1}{\sqrt{\alpha_{p_1}\alpha_{n_2}\beta_1\beta_2}} \right] \tag{21}$$

For real values of the parameters on the right hand sides of (20) and (21), which are given in Section 4 (see Eqs. (22)–(24)), the error angles are of several degrees or less. Eqs. (18)–(22) reveal that the error angles can be minimized via selecting the resistance values much smaller than the parasitic resistances of z terminal, and fulfilling the symmetry condition (17). It is interesting that the parasitic phase shift of voltage signals is governed by the parasitic R_z resistance of CDBA no. 1 while the phase error of current signals depends on the R_z of CDBA no. 2.

Note that the above error angles increase with decreasing oscillation frequency, which figures in the denominators of the dominant terms in (18) and (19). This phenomenon can be explained such that the 90° phase shift between the generated signals is accomplished by the integrators, and that the parasitic R_z resistance in parallel to the working capacitance causes an additional phase error, which is dominant just at low frequencies, where the capacitive reactance increases. In order to make this effect negligible for low oscillation frequencies, the active element should be designed with the parasitic resistance of the z terminal as high as possible. Techniques like cascoding and regulated cascoding can be used to achieve higher output resistances at the z terminal of transistor-level implementations.

On the other hand, the above analysis does not include additional effects caused by the finite bandwidth of the active elements. As shown in Section 4, the actually measured error angles can be different than the values estimated via (19) and (21). The reason consists in that, for higher oscillation frequencies, the additional phase shift caused by the current differencing unit (CDU) is rather low, thus without the potency to substantially influence the oscillation frequency, but comparable in size with the error angle described by (19).

Since the analytical derivation of the above influence on the error angle δ_I is complicated due to the large number of frequency-dependent terms in (15), such an analysis will be done only for the error angle δ_V. Note that if the symmetry condition (17) is fulfilled, then the procedure can be utilized also for the estimation of δ_I.

For frequency-dependent current gain α_{p1} of the CDU and voltage gain β_1 of the output buffer, Eq. (16) can be rewritten as follows:

$$\frac{V'_{o2}}{V'_{o1}} = \frac{R'_1}{R_{z1}} \frac{1 + j\omega'_0 C'_1 R_{z1}}{\beta_1(\omega)\alpha_{p_1}(\omega)} \tag{22}$$

Then the phase shift φ_{21} between the output signals V'_{o2} and V'_{o1} is

$$\varphi_{21} = \tan^{-1}(\omega'_0 C'_1 R_{z1}) - \varphi_{p1} - \varphi_{\beta1} \tag{23}$$

where φ_{p1} and $\varphi_{\beta1}$ are additional phase shifts generated by the CDU and buffer.

The error angle δ_V is as follows:

$$\delta_v = 90° - \varphi_{21} = 90° - \tan^{-1}(\omega_0' C_1' R_{z1}) + \varphi_{p1} + \varphi_{\beta1}$$

$$= \tan^{-1}\left[\frac{1}{\omega_0' C_1' R}\right] + \varphi_{p1} + \varphi_{\beta1} \qquad (24)$$

Comparing (24) and (19), one can conclude that the CDU and buffer of active component no. 1 (see Fig. 2) modify the resulting phase shift between two generated signals. Without this influence, typically for low oscillation frequencies, the error angle (19) is positive. However, φ_{p1} and $\varphi_{\beta1}$ are negative since they represent delays caused by the lowpass character of the CDU and buffer transfer functions in such a way that the resulting error angle can be lower than that from (19) for certain oscillation frequencies (see Section 4 for more details).

Note that only the parameters of the subcircuit associated with ZC-CG-CDBA no. 1 are present in (24) for computing the error angle. However, the remaining part of the oscillator affects this error too, since it modifies the oscillation frequency, which also appears in (24).

4. Experimental results

As shown in [18], ZC-CG-CDBA can be implemented by means of current-controlled current conveyors CCCII+. The final implementation in [18] with commercial "diamond transistors and buffers" OPA860 is optimized for minimizing the input resistances of the p and the n terminals and reducing the current offset using the so-called degeneration resistors. This ZC-CG-CDBA implementation was selected for the experimental verification just because of a proof in [18] that it really works and that the behavior of the constructed specimen corresponds well with the behavior of the Spice model from the OPA860 manufacturer.

For experimental verification as well as PSPICE simulations, the ZC-CG-CDBA was implemented exactly the same as in [18] (as redrawn in Fig. 3). The quiescent current of the specimen, 80 mA, is rather high due to the use of several OPA860. It can be considerably reduced for concrete on-chip implementations.

The diamond transistor operates as a CCII+ with the x terminal (emitter) parasitic resistance, which is equal to the reciprocal value of the internal transconductance g_m. That is why the I_p current, flowing to the emitter of T_0, also flows to the collector. As shown in Fig. 3, the emitter current of T_1 must be then a difference of currents I_p and I_n. The difference current $I_p - I_n$ is also conveyed to the collector of T_1. Due to the high-impedance base terminal of T_3, this current flows through the degeneration resistor R_{e2}, causing a voltage drop $(I_p - I_n) R_{e2}$. This voltage then drives the transistor T_3, with its emitter and also collector current being defined by this voltage and degeneration resistance R_{e3}. As a result, the ratio of currents I_z and $I_p - I_n$, i.e. the current gain α, can
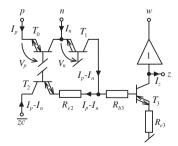
be adjusted by the ratio of degeneration resistances R_{e2}/R_{e3}. This statement is accurate when degeneration resistances are much higher than $1/g_m$. For $\alpha = 1$, their values were chosen 1 kΩ. For $\alpha < 1$, R_{e2} was fixed at 1 kΩ and R_{e3} was increased accordingly. Details about the reason for using R_{b3} are given in [18].

The typical small-signal real parameters of such implemented ZC-CG-CDBA are as follows [18]:

$$R_p = R_n \approx 10\,W, \quad R_z \approx 51.2\,kW$$

$$C_z \approx 4.1\,pF, \quad R_{zc} \approx 54\,kW, \quad C_{zc} \approx 2\,pF \qquad (25)$$

In addition, the following values of current and voltage gains were measured:

$$\alpha_{pc} \approx 0.937, \quad \alpha_{nc} \approx 0.951, \quad \beta \approx 0.991 \qquad (26)$$

The values α_p and α_n depend on the theoretical values of current gain $\alpha = R_{e2}/R_{e3}$ according to Fig. 4. The approximate modeling of this dependence is as follows:

$$a \approx 0.932a, \quad a_n \approx 0.946a \qquad (27)$$

Note that these values, which were measured for one specimen of the ZC-CG-CDBA, are subject to the variation of circuit components and thus they represent only a sample of possible real values.

For $R_{e2} = R_{e3} = 1$ kΩ, which represents the highest value $\alpha = 1$, and also the highest value of the oscillation frequency, the bandwidth of the current differencing unit is more than 30 MHz. However, the current gains decrease by 1% at thea frequency of less than 6 MHz, and the parasitic phase shift at 3 MHz is more than 6°. These numbers illustrate the fact that one must bear in mind the above influences manifested in the range of >0 oscillation frequencies above ca. 1 MHz, when the FO decreases below its theoretical value and the error phase shift between the orthogonal signals are also modified.

It follows from Fig. 2 that, in contrast to the definition in Fig. 1, the difference in the current $I_p - I_n$ flows into, not out of the zc terminal. The utilization of active elements with inverted zc terminals requires a modification of the schematic in Fig. 2. There are two basic methods illustrated in Fig. 5(a) and (b).
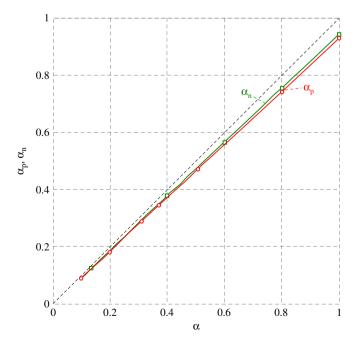

Fig. 3. Implementation of ZC–CDBA with minimizing the p and n resistances and offset reduction; see [18] for more details.

Fig. 4. Measured dependence of ZC-CG-CDBA current gains on the ratio of resistances $\alpha = R_{e2}/R_{e3}$.
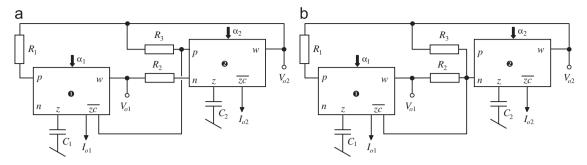
Fig. 5. Two modifications of the oscillator from Fig. 2 for ZC-CG-CDBAs with inverted copies of z-current.

In the oscillator in Fig. 5(a), the inverted copy of z-terminal current is simply led not to the n but to the p terminal of ZC-CG-CDBA no. 2. Then the sign of the corresponding loop gain is unchanged.

In the oscillator in Fig. 5(b), R_3 is connected not to the p but to the n terminal of ZC-CG-CDBA no. 2. In contrast to the original circuit from Fig. 1, the signs of the two loop gains in the oscillator are now interchanged. This modification does not change the theoretical FO in Eq. (4). The condition of oscillation (3) is now modified as follows:

$$R_3 \geq R_1 \tag{28}$$

The circuit in Fig. 5(b) has two advantages:

(1) The p terminal of ZC-CG-CDBA no. 2 is not used. Then the transistor T_0 in Fig. 3 can be omitted, and the oscillator specimen can be constructed more economically.
(2) A simple AGC (Automatic Gain Control) circuit can be implemented for automatic regulation of the oscillation condition: R_3 is replaced by a photoresistor, which is a part of the opto-coupler, the latter being excited by the rectified voltage output of the oscillator. For decreasing oscillations, the light emitted by the internal LED becomes reduced and thus the resistance R_3 is increased, stimulating the growing loop gain. In the circuit in Fig. 5(a), the AGC implementation with the same opto-coupler would be more complicated.

An error analysis of the oscillation frequency of the modified circuits in Fig. 5 reveals that the practical formula (13) is valid also for the oscillator in Fig. 5(a). This formula can also be used for the circuit in Fig. 5(b), but only after replacing the value

$$R'_2 = R_2 + R_{n2}$$

by

$$R'_2 = R_2 + R_{n2}(1 + R_2/R_3) \tag{29}$$

As a concrete effect, the oscillation frequency of the circuit in Fig. 5(b) will be lower in comparison to the circuit in Fig. 5(a) due to the increased value of the modified resistance R_2. However, this decrease will be only up to ca. 1% for the parameters considered below.

Based on the ZC-CG-CDBA implementation in Fig. 3, the oscillator in Fig. 5(b) was manufactured as shown in Fig. 6.

The oscillation condition is accomplished via the VTL5C4 opto-coupler, employing a photo-resistor whose resistance is controlled by the amplitude of generated waveforms, as in [17,20]. The opto-coupler is excited from the output of a fast and precise RMS-to-DC converter, designed according to [23]. The sinusoidal voltage drop across the potentiometer, connected to the Z-copy terminal of ZC-CG-CDBA no. 2, is converted by the RMS-to-DC block to DC voltage for exciting the internal LED of the opto-coupler. The 1.5 nF capacitor removes the prospective offset
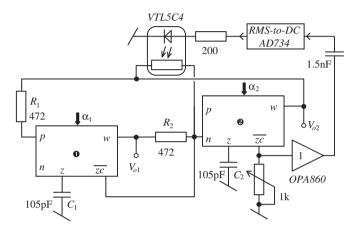

Fig. 6. Oscillator specimen including the AGC employing opto-coupler VTL5C4.

voltage. The potentiometer enables adjusting the magnitude of generated waveforms, and it can also be used for sensing the current output.

The oscillator was manufactured with the following parameters of passive components:

$$R_1 = R_2 = R = 472\,\Omega, \quad C_1 = C_2 = C = 105\,\text{pF} \tag{30}$$

According to (4) and (8) and for $\alpha_1 = \alpha_2 = \alpha = 1$, the corresponding theoretical value of the oscillation frequency is 3.21 MHz. The total capacitance measured between the z terminal of each CDBA and the ground was 110 pF, indicating an additional parasitic capacitance of 5 pF. Considering also the decrease of current gains due to the non-idealities of active components according to (27), the oscillation frequency computed from (4) is 2.88 MHz. After evaluating Eqs. (10) and (13) (with the help of Eq. (29)), which also model the influence of other error factors, we get practically the same results from both equations, 2.76 MHz. The generated waveforms, shown in Fig. 7, have a repeating frequency of 2.75 MHz. This proves the correctness of the non-ideal analysis from Section 3. The THD values of the signals generated were 0.26% and 0.21%. All the measurements were performed using the HANDYSCOPE HS3-AWG-100 USB oscilloscope.

During the measurements, α was modified and the expected proportional dependence of the oscillation frequency, the THD, and the phase error angle were evaluated. In addition, the measured waveforms were exported to PSpice for subsequent processing and for a better comparison of measured and ideal results and results estimated by the error analysis from Section 3. The phase shifts between the generated signals were computed via the PSpice Fourier analysis, which is more precise than sensing them from the waveforms. The results are shown in Figs. 8 and 9.
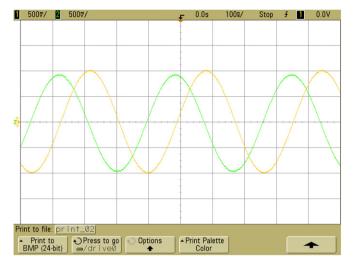
Fig. 7. Signals generated at outputs V_{o1} and V_{o2} of QO in Fig. 6, with a repeating frequency of 2.75 MHz.
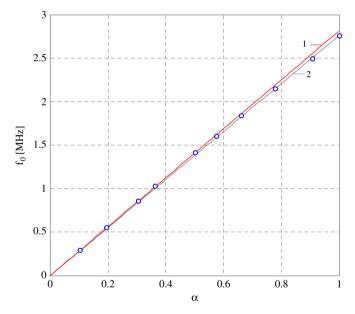

Fig. 8. Oscillation frequency versus $\alpha_1 = \alpha_2 = \alpha$: (1) theoretical values according to (4), considering measured values of z-terminal capacitances and non-ideal current gains (27), and (2) values according to (13) and (29), (o) measured values.

Fig. 8 shows the f_0 versus α plots, comparing the theoretical curves generated by Eqs. (4) and (13) and the measured values. Note that the measured frequencies are in very good agreement with the models derived in Section 3.

According to formula (21), the parasitic phase shift between the generated signals decreases with increasing oscillation frequency. However, the values measured indicate an additional phase shift caused by ZC-CG-CDBAs. The data measured are in good agreement with the curve computed from Eq. (24). Here, the phase shift generated by the voltage buffer from OPA860, which was used in the specimen, is neglected since its bandwidth is 1.6 GHz. The phase shift caused by the CDU was computed via its single-pole model with a cutoff frequency of 35 MHz. Note that such a model describes the reality only approximately because the I_z/I_p transfer function is of higher order. It is shown in Fig. 9 that the oscillator specimen generates precise quadrature signals for oscillation frequencies of about 1 MHz.
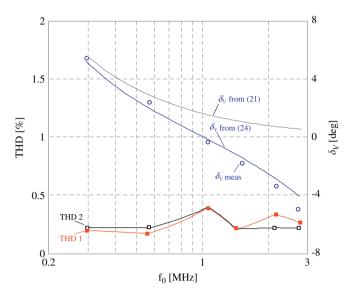

Fig. 9. THD of generated signals at output V_{o1} (THD 1) and V_{o2} (THD 2), measured and estimated phase errors (δ_v means, δ_v from (21) and δ_v from (24)) versus frequency.

5. Concluding remarks

A first of its kind 3R-2C quadrature sinusoidal oscillator is proposed, which can simultaneously provide quadrature voltage outputs and explicit quadrature current outputs. The circuit not only serves as a new application of the recently proposed building block, namely the Z-copy controlled-gain current differencing buffered amplifier (ZC-CG-CDBA), but more importantly it proves to be a unique oscillator suitable to be used in both voltage- and current-mode applications. The non-ideal analysis of the proposed circuit has been carried out and experimental results have confirmed its workability.

Acknowledgment

References

[1] S.S. Gupta, R. Senani, New single resistance controlled oscillators employing a reduced number of unity gain cells, IEICE Electronics Express 16 (2004) 507–512.
[2] V.K. Singh, R.K. Sharma, A.K. Singh, D.R. Bhaskar, R. Senani, Two new canonic single-CFOA oscillators with single resistor controls, IEEE Transactions on Circuits and Systems II 52 (2005) 860–864.
[3] S.S. Gupta, R. Senani, State variable synthesis of single resistance controlled grounded capacitor oscillators using only two CFOAs, Proceedings of IEE-Circuits, Devices and Systems 145 (1998) 135–138.
[4] A.M. Soliman, Synthesis of grounded capacitor and grounded resistor oscillators, Journal of the Franklin Institute 336 (1999) 735–746.
[5] W. Tangsrirat, W. Surakampontorn, Single-resistance-controlled quadrature oscillator and universal biquad filter using CFOAs, AEU— International Journal of Electronics and Communications 63 (2008) 1080–1086.
[6] W. Tangsrirat, D. Prasertsom, T. Piyatat, W. Surakampontorn, Single-resistance-controlled quadrature oscillator using current differencing buffered amplifiers, International Journal of Electronics 95 (2008) 1119–1126.
[7] S. Maheshwari, I.A. Khan, Novel single resistance controlled oscillator using two CDBAs, Journal of Active and Passive Electronic Devices 2 (2007) 137–142.
[8] S. Özcan, A. Toker, C. Acar, H. Kuntman, O. Çiçekoglu, Single resistance-controlled sinusoidal oscillators employing current differencing buffered amplifier, Microelectronics Journal 31 (2000) 169–174.

[9] J.-W. Horng, Current differencing buffered amplifiers based single resistance controlled quadrature oscillator employing grounded capacitors, IEICE Transactions on Fundamentals E85-A (2002) 1416–1419.

[10] C.M. Chang, B.M. Al-Hashimi, H.P. Chen, S.H. Tu, J.A. Wan, Current mode single resistance controlled oscillators using only grounded passive components, Electronics Letters 38 (2002) 1071–1072.

[11] W. Jaikla, M. Siripruchyanun, J. Bajer, D. Biolek, A simple current-mode quadrature oscillator using single CDTA, Radioengineering 17 (2008) 33–40.

[12] A. Lahiri, New current-mode quadrature oscillators using CDTA, IEICE Electronics Express 6 (2009) 135–140.

[13] A. Lahiri, Explicit-current-output quadrature oscillator using second-generation current conveyor transconductance amplifier, Radioengineering 18 (2009) 522–526.

[14] S.S. Gupta, R. Senani, Realisation of current mode SRCOs using all grounded passive elements, Frequenz 57 (2003) 26–37.

[15] S.S. Gupta, R.K. Sharma, D.R. Bhaskar, R. Senani, Sinusoidal oscillators with explicit current output employing current-feedback op-amps, International Journal of Circuit Theory and Applications 35 (2010) 131–147.

[16] D. Biolek, A.U. Keskin, V. Biolkova, Grounded capacitor current mode single resistance-controlled oscillator using single modified current differencing transconductance amplifier, IET Circuits, Devices and Systems 4 (2010) 496–502.

[17] J. Bajer, D. Biolek, Digitally controlled quadrature oscillator employing two ZC-CG-CDBAs, in: Proceedings of the International Conference on EDS-IMAPS 2009, Brno, Czech Republic, 2009, pp. 298–303.

[18] D. Biolek, J. Bajer, V. Biolkova, Z. Kolka, M. Kubicek, Z copy-controlled gain-current differencing buffered amplifier and its applications, International Journal of Circuit Theory and Applications 39 (2011) 257–274. doi:10.1002/cta.632.

[19] D. Biolek, R. Senani, V. Biolkova, Z. Kolka, Active elements for analog signal processing: classification, review, and new proposals, Radioengineeing 17 (2008) 15–32.

[20] J. Bajer, A. Lahiri, D. Biolek Current-mode CCII+ based oscillator circuits using a conventional and modified wien-bridge with all capacitors grounded, in: Proceedings of the International Conference on EDS-IMAPS 2010, Brno, Czech Republic, pp. 5–10.

[21] D.R. Bhaskar, R. Senani, New CFOA-based single-element-controlled sinusoidal oscillators, IEEE Transactions on Instrumentation and Measurement 55 (2006) 2014–2021.

[22] A.S. Elkawil, Systematic realization of low-frequency oscillators using composite passive–active resistors, IEEE Transactions on Instrumentation and Measurement 47 (1998) 584–586.

[23] AD734: 10 MHz, Four-Quadrant Multiplier/Divider. Analog Devices, Datasheet, Rev. E, 2011, p. 16, Fig. 34.